RETINAL THICKNESS MEASUREMENTS USING OPTICAL COHERENC TOMOGRAPHY

MADHUMITHA V[1], P. APARNA[2] & KENDAGANNA SWAMY[3]

[1,2]Department of Instrumentation Technology, R.V College of Engineering, Bangalore, Karnataka, India

[3]Assistant Professor, Department of Instrumentation Technology, R.V College of Engineering, Bangalore, Karnataka, India

ABSTRACT

Optical coherence tomography (OCT) has become a conventional occular imaging technique which can be used in the diagnosis of glaucoma by measuring the retinal nerve fiber layer (RNFL) thickness. This paper reviews various techniques used to measure the RNFL thickness. The Gaussian Mixture Model (GMM) makes use of a kernel and cluster masks which detects eight retinal layers with nine boundaries. Automated Layer Segmentation model uses iterative polynomial smoothing procedure and detects five retinal layers accurately. The Markov Boundary model uses edge detection kernel which detects the outer and inner retinal boundaries along with retinal landmarks. GMM detects more number of retinal layers thereby more information is obtained for better pathological and ocular diagnosis.

KEYWORDS: Glaucoma, Optical Coherence Tomography (OCT), OCT Layer Segmentation, Boundary Detection, Edge Detection, Retina, Retinal Nerve Fiber Layer (RNFL), Kernel, Filter

1. INTRODUCTION

Optical coherence tomography (OCT) is an optical signal acquisition and processing method. As it is a noninvasive real time imaging tool, with micrometer-scale resolution, it is the preferred method of imaging nerve tissues such as retina. OCT offers higher resolution than high-frequency ultrasound. Ophthalmology has been one of the main application areas of Optical Coherence Tomography [1] since its invention in 1991. OCT allows a direct visualization of the retina and its layered structure. Measurement of the thickness of retinal nerve fiber layer helps in the diagnosis of ocular diseases like glaucoma, characterised by the loss of the retinal nerve fiber.

This review paper has been organized as follows. This section, continues with a discussion of the relevant ophthalmology and explains the general theory behind OCT. Section II deals with the various techniques that are involved in the detection of RNFL. The principle of these techniques along with the experimental implementations and results are discussed in the section. Section III presents the results by comparing the techniques discussed in section II and Section VII offers some concluding remarks.

1.1. Ophthalmology

So that the reader will understand the clinical significance of the problem at hand, this section briefly overviews the relevant ophthalmology. The posterior portion of the eye is a hollow sphere filled with the clear, jelly-like vitreous humor and the retina is a thin film of nervous tissue lining the inner surface of the posterior ocular wall [2]. The eye's radial geometry makes the terms *inner* (toward the centre of the eye) and *outer* useful for orientation within the retina. Just outside the retina lies the choroid, a tissue whose dense network of blood vessels renders it opaque to infrared light.

The fovea is a small depression in the retinal surface, at the location corresponding to the centre of the visual field. Many diseases affecting vision cause changes in retinal thickness, with macular edema being a prominent example.

Macular edema is the primary cause of vision loss in diabetics [3] and tracking retinal thickness changes over time is important in determining the appropriate treatment [4]. Currently, the slit lamp bio microscope is the most commonly used clinical device for assessing retinal thickness. With it, the ophthalmologist views a magnified, stereo image of the retina illuminated obliquely by a narrow slit of light and subjectively assesses thickening.

Though thickening above a certain threshold is readily detected based on gross appearance, there is no measuring scale for precise quantification. This lack of quantification makes it difficult to track changes over time. OCT's quantitative nature permits accurate and precise measurements of patient changes.

1.2. General OCT Theory

An OCT system is essentially a Michelson interferometer; the two light paths are called the reference path and the imaging path and the subject's eye terminates the imaging path [5].
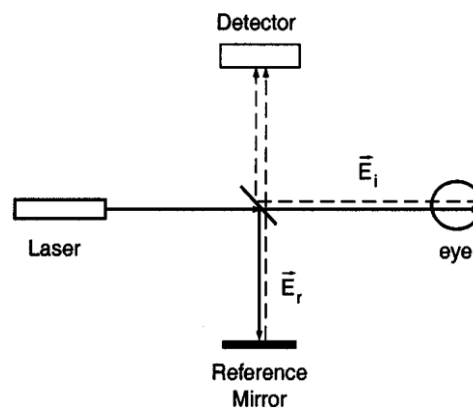

Figure 1: Schematic Drawing of the OCT Emphasizesg how it is Essentially a Michelson Interferometer the Outgoing Light Paths are Solid Lines, While Reflected Light is Drawn as Dashed Lines [11]

Figure 1 illustrates this concept with a schematic drawing of an OCT system. In the figure, the reflected light is represented by the electric field vectors, in the imaging path and in the reference path. Solid lines depict outgoing light and dashed lines depict reflected light. To understand OCT operation, one should first imagine the eyeball in Figure 1 replaced by a mirror located exactly 1 m from the beam splitter. The reference mirror in this thought experiment is initially placed 5 m from the beam splitter and then slowly moved outwards to a distance of 1.5 m.

2. RNFL DETECTION METHODS

RNFL thickness is an important parameter for clinical and pathological analysis of ocular diseases. Various techniques have been adopted in detecting the thickness. In this paper four such methods have been reviewed namely Gaussian mixture model, Automated layer segmentation (Time and Frequency Domain), and Markov boundary model.

2.1. Gaussian Mixture Model

This method uses a segmentation algorithm based on an intelligent tracking kernel and a clustering mask based on the Gaussian mixture model (GMM). The kernel extracts boundaries by moving and matching its faces with locally clustered images generated by GMM clustering. The cluster-guided motion of the kernel enables sensitive classification of structures on a single-pixel scale.

This system targets seven major retinal boundaries. Then, using peak detection, additional two simple boundaries are easily grabbed in regions where their distinct features emerge sufficiently in the limited space remaining after the previous segmentation.
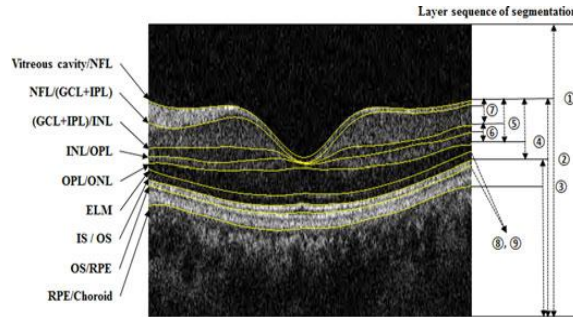
**Figure 2: Image Showing Retinal Boundaries and Layer Segmentation Sequence.
The Boundaries are Segmented Progressively within Each Region of the Sequence [12]**

An image of segmented retinal layers is shown in Figure 2. The layers include a vitreous cavity, nerve fiber layer (NFL), ganglion cell layer with an inner plexiform layer (GCL + IPL), inner nuclear layer (INL), outer plexiform layer (OPL), outer nuclear layer (ONL), external limiting membrane (ELM), inner segment (IS), outer segment (OS), retinal pigment epithelium (RPE), and choroid. For segmentation, the vitreous cavity/NFL, IS/OS, RPE/choroid, OPL/ONL, (GCL+IPL)/INL, INL/OPL, NFL/(GCL+IPL), ELM, and OS/RPE boundaries are tracked in the sequence _1 to _9. The segmentation layer sequence is based on the level of difficulty associated with the detection of each layer.
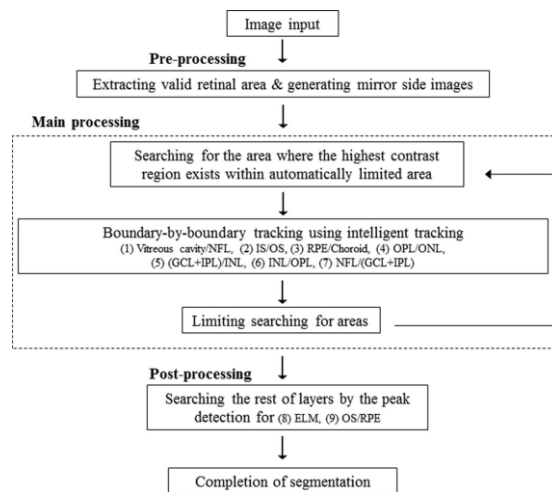

**Figure 3: Flowchart Showing the Algorithm Steps. In the Main Processing Step, Seven Retinal
Boundaries are Tracked Using Intelligent Tracking. The Other Two Boundaries Are Detected
Using Simple Edge Detection Based on the Previously Tracked Boundary Indices [12]**

A flowchart of the algorithm framework is shown in Figure 3. The algorithm consists of three parts: pre-processing, main processing, and post-processing. Pre-processing is performed to prepare the images. The seven boundaries are then segmented in the main processing step. The highest contrast region is found and used to define the start of each layer, and the kernel system tracks each boundary. After one boundary is tracked, the algorithm limits the region for other boundary tracking and searches for the next highest region. These generalized layer segmentation procedures are used for the main processing steps. Once the first seven boundaries have been detected, ELM and OS/RPE boundaries are extracted using the peak detection method in the post-processing step. The peak detection method is used here because these are simple boundaries that can be easily detected once the confidence region has been determined in the main processing step. Thus, the total system is operated in hybrid modes.

The pre-processing stage of this algorithm involves the preparation and processing of the input images so that they can be efficiently analyzed. Extraction is performed only in specific areas, and mirror side images are generated. A mirror image is also needed for image compensation of each side. When the kernels are applied, both side areas are expanded to

contain the virtual image. This allows the side columns to be perfectly covered and tracked. The automated system must be robust against noise factors to allow stable and sensitive segmentation. To ensure that the system is equipped with these capabilities, a kernel concept is used. Using a regular rectangular kernel, the pixels of interest and their location in each layer are defined. The ratio of the kernel size can generally be optimized according to the width: height ratio of the image. Generally the height of the kernel is smaller than the width.

Once the size of the kernel has been determined, GMM clustering is performed to classify the pixels according to each pixel's layer. It separates the components into designated groups. The classification scheme uses the pixel intensity and row value for each location because retinal layer segmentation is directed upward and downward. Therefore, the GMM is sensitive to changes in the pixel intensity and image contrast levels. This characteristic is used in the algorithm to classify the pixels as sensitively as possible.
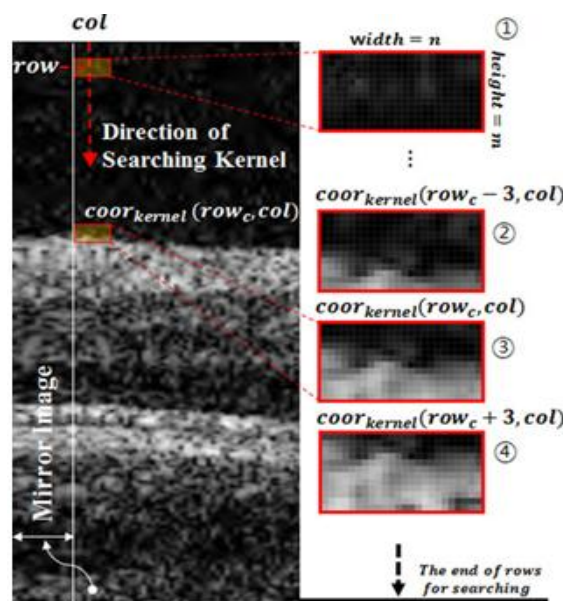
Figure 4: Images Showing how the Interface Layers are Found Using the Searching Kernel. Red Kernel Passes Vertically Down from the First Column of the Original Image to Find the Areas with the Highest Contrast [12]

Maximum kernel contrast is required to find the starting positions of the boundaries in the columns covered by the kernel. The kernel then moves downward and compares the change in the image contrast of the pixels as seen in Figure 4. To precisely calculate the contrast change and relate this to the structures in the image, the pixels in the kernel are processed using GMM clustering so that as the kernel approaches the layer interface, the intensity difference between adjacent pixels increases. To determine the interface, this method uses the absolute mean intensity difference between two clusters. The pixels in the tracking kernel and the cluster masks are matched.

The position of the kernel needs to be adjusted to the middle of the structures. The kernel mask can move up and down with respect to its original position and can also rotate above the clustering mask. The matching pixels are counted at each position and a new kernel position is obtained. The positioning procedure is then repeated so that the new kernel is located in its optimum position. Finally, through continuous repetition of this process until the last column, the boundary line along the layer interface is formed.

The segmentation algorithm was implemented using MATLAB, and the datasets were processed using a personal computer (CPU: Core i3 3.10 GHz, RAM: 2 GB). OCT retinal images in the fovea were provided by Topcon 3D-2000. The images were approximately 700×1200 pixels in size, and a kernel size of 12×24 pixels was initially set for the extraction.
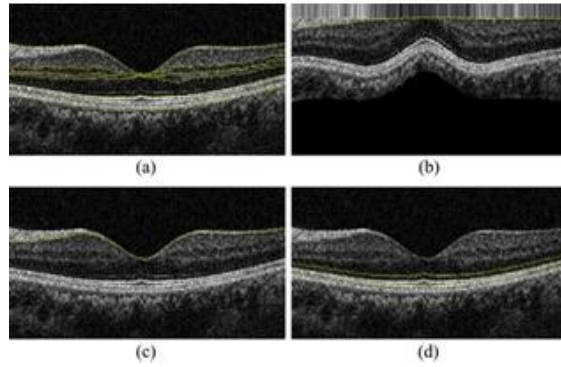
Figure 5: Segmentation Steps. (a) Vitreous Cavity/NFL, (GCL+IPL)/INL, INL/ OPL, OPL/ONL, IS/OS, and RPE/Choroid Boundaries are Segmented Using Intelligent Tracking System. (b) NFL/(GCL+IPL) is Segmented in the Morphologically Transformed Image to Support the Disappearing NFL Layer by Dragging Pixels up onto the Designated Vitreous Cavity/NFL in Every Column. (c) Tracked NFL/(GCL+IPL) Boundary in Transformed Image is Rearranged by Restoring Vitreous Cavity/NFL Boundary's Coordination. (d) ELM and OS/RPE are Detected by Simple Peak Detection in Confident Regions for Other Boundaries. [12]

Figure 5(a) shows the results of image processing using the tracking kernel for the six different boundaries. The NFL/(GCL+IPL) boundary was found by the same tracking kernel used above. This detected line on the transformed image is shown in Figure 5(b). After the NFL/(GCL+IPL) boundary was fully tracked, the image was recovered to the original form as shown in Figure 5(c). A sample image of the detected ELM and OS/RPE boundaries is shown in Figure 5(d). All the boundary lines in Figure 6 occupy only one pixel per a boundary in a column and are displayed as yellow solid lines. This result demonstrates the accuracy of this segmentation method.

2.2. Automated Layer Segmentation

In the proposed technique, an OCT image is first cut into multiple vessel and non-vessel sections by the retinal blood vessels that are detected through an iterative polynomial smoothing procedure. The non-vessel sections are then filtered by a bilateral filter and a median filter that suppress the local image noise but keep the global image variation across the retinal layer boundary. Finally, the layer boundaries of the filtered non-vessel sections are detected, which are further classified to different retinal layers to determine the complete retinal layer boundaries.

Based on the dimension of the image information used, there are 3 methods for retinal layer boundary detection:
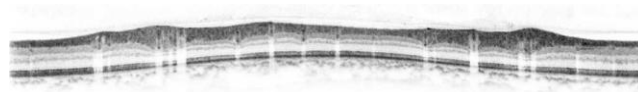

Figure 6: Example OCT Image of the Peripapillary Region of the Optic Disc. [10]

- D uses the gradient peak detection

- D uses edge detection and level sets

- D uses optimal graph search techniques [1].

The unique features of the proposed technique are:

  o From the OCT, the initially detected retinal blood vessels are separated into multiple vessel and non-vessel sections.

  o The layer boundary of the non-vessel sections can be classified into specific retinal layers for interpolation using the prior knowledge of the relative image gradients across different retinal layer boundary which have a fixed order.

o Bilateral and median filtering techniques are used for smoothing and suppressing local noise respectively.

o 5 layers are obtained after segmentation, which includes the retinal nerve fiber layer (RNFL).

The retinal layers have to be labelled automatically. For this, the OCT image as illustrated in Figure 6 is first cut into multiple vessel and non-vessel sections by the retinal blood vessels. Smoothing technique is used here.
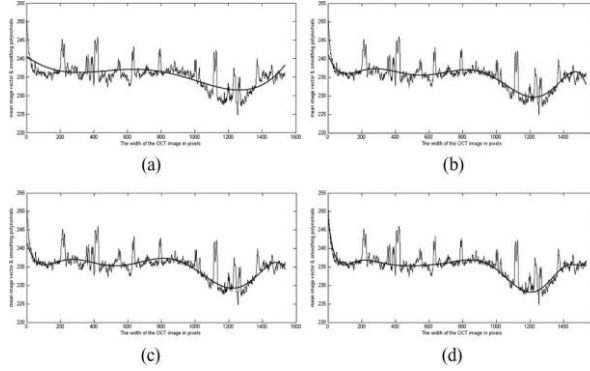

Figure 7: Retinal Blood Vessel Detection. (a)–(d) Light Graph Shows the Mean Image Vector of the OCT Image in Figure 6 and the Bold and Smooth Graphs Show the Smoothing Polynomials Fitted in Increasing Iterations [10]

The vessel sections can thus be located through an iterative

Polynomial smoothing procedure described in Algorithm I.

Algorithm I

Step 1: *Fit a polynomial P of order N (initial polynomial order) to all sampling data as specified in (1).*

Step 2: *Evaluate the maximum fitting error (defined below). Remove the sampling point with the maximum fitting error, if the error is larger than a predefined threshold T.*
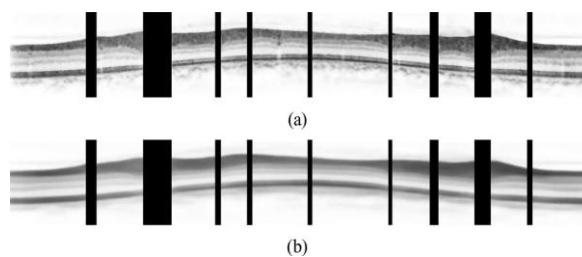

Figure 8: OCT Filtering. (a) OCT Image after Bilateral Filtering. (b) OCT Image after Median Filtering of the OCT Image in (a) [10]

Step 3: *Refit a smoothing polynomial Pi of order Ni as specified in (2) to the remaining sampled data.*

Step 4: *Repeat Steps 2 and 3 iteratively until the maximum fitting error is smaller than the predefined threshold or the remaining data points are smaller than Ni + 1.*

As described in Step 3, the polynomial order is gradually increased to ensure that the sampling point with larger deviation is removed earlier. The polynomial order is set initially at 6 (i.e., $N = 6$) and adapt it as follows:

$$Ni = N + frnd(kp\ i),\ i = 1, \ldots, n \tag{1}$$

Where *frnd*(·) and *i* denote a rounding function and the iteration number. Parameter *kp* is set at 0.1, which controls

the increase speed of the polynomial order. The predefined threshold T specifies the maximum fitting error allowed and it can be empirically set between 2 and 4 (the fitting error is the absolute difference between the sampled mean image intensity and the fitted smoothing polynomial shown in Figure 7). The bold and smooth graphs in Figure 7(a)–(d) show the smoothing polynomials fitted in the first, tenth, twentieth, and thirty seventh iteration, respectively. As Figure 7 shows, the polynomials fit closer to the mean image vector of the non-vessel sections during the smoothing process.

The vessel sections can thus be detected through the global thresholding [8] of the difference between the mean image vector and the final smoothing polynomial shown in Figure 7(d).

The non-vessel sections are removed by bilateral filtering. A median filter is used to suppress the local noise and to also keep the image variation across the retinal layer boundary. A bilateral filter may not remove noise of large size as shown in Figure 8(a). The filter window needs to be set with care due to specific OCT characteristics. In particular, the window height cannot be too large; otherwise, the image variation across the boundary of certain thin OCT layers will be smoothed away completely. The window width can instead be much larger than the window height due to the roughly horizontal orientation of the OCT layers. A rectangle window is used and the window height is set at 34.2 μm because retinal layers are usually thicker than 30.4 μm in OCT images. Figure 4(b) shows the OCT image filtered by a median filter of 34.2 μm × 193.8 μm.
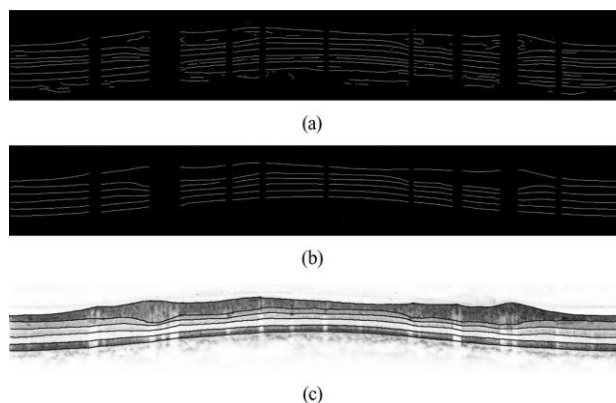

(a)

(b)

(c)

Figure 9: Retinal Layer Boundary Detection. (a) Edges Detected from the Non-Vessel OCT Sections in Figure 4(b) (b) Retinal Layer Boundaries Identified from the Edges in (a). (c) Finally Determined Retinal Layer Boundary [10]

Retinal layer boundary can thus be detected from the filtered OCT images. The layer boundaries of the non-vessel sections are first detected and then classified into different specific OCT layers. Layer boundaries of the vessel sections are then determined through linear interpolation of the layer boundaries detected from the neighboring non-vessel sections. For each filtered non-vessel section, the edges are first detected using Canny's edge detector [9] and then the retinal layer boundaries from the detected edges are identified. For the filtered OCT image in Figure 8(b), Figure 9(a) shows the image edges detected by Canny's edge detector and Figure 9(b) shows the identified layer boundary of the non-vessel section that can be classified to specific OCT layers based on their relative position within each non-vessel section.

The layer boundary of vessel sections can be further determined through interpolation of the corresponding layer boundary of neighbouring non-vessel sections. For the OCT image in Figure 6, Figure 9(c) shows the finally determined retinal layer boundary.

For each test OCT image, multiple retinal layer boundary pixels are first labelled by medical experts and a complete retinal layer boundary is determined through spline fitting of the labelled pixels. The thickness of a retinal layer is determined by the distance between the fitted upper and lower layer boundaries, which will be used as a reference standard to evaluate the layer thickness determined by the proposed method. It should be noted that

Table 1: Summary of Mean and Standard Deviation of RNFL Thickness Error (in *M*m) for 16 Oct Images [10]

|	1st Visit	2nd Visit	3rd Visit	4th Visit
Subj. 1	2.67 ± 1.37	2.14 ± 1.27	2.92 ± 1.44	2.78 ± 1.51
Subj. 2	1.96 ± 0.87	2.93 ± 1.12	2.38 ± 1.06	2.77 ± 1.43
Subj. 3	5.35 ± 3.02	4.89 ± 3.11	5.24 ± 2.91	4.94 ± 3.17
Subj. 4	2.56 ± 2.08	2.79 ± 1.83	2.99 ± 2.06	2.88 ± 1.91

Only the RNFL thickness that is widely used for glaucoma diagnosis is evaluated. Table 1 shows the average RNFL thickness error for the OCT of the four subjects. As shown in Table 1, the proposed method is repeatable for the OCT in different visits demonstrating an accurate and reliable RNFL thickness assessment. Experiments over OCT for four subjects show that the proposed technique segments an OCT image into five retinal layers accurately.

2.3. Markov Boundary Model

The boundary-detection system presented here uses a one-dimensional edge-detection kernel to yield edge primitives. These edge primitives are rated, selected, and organized to form a coherent boundary structure by use of a Markov model of retinal boundaries as detected by OCT.

In designing a retinal boundary detector, in this model retinal anatomy and the principles of OCT operation are used to make various assumptions about the image boundary characteristics. To begin, the normal retina has smooth boundaries without discontinuities or gaps and, within OCT images, the inner boundary is always above the outer boundary.

However, it takes about 1-s to acquire all 100 A-scans, long enough for involuntary eye motion to occur during the process. Patient motion can cause artefacts ranging from undulations to apparent breaks in the retinal image. Because the OCT acquires each A-scan individually, one-dimensional (1-D) edge detection to each image column individually is applied, similar to Thune et al. [7].
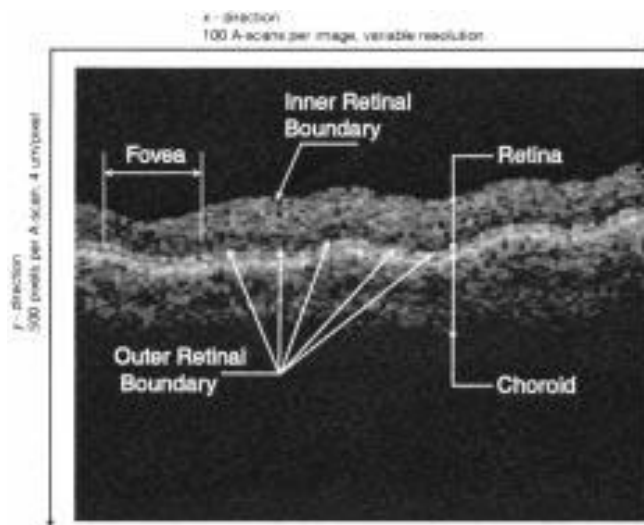

Figure 10: Sample OCT Scan from the Set of Training Images with Anatomical Features Labelled [11]

In Figure 10 the inner and outer retinal boundaries along with other retinal landmarks and the directions along which A-scans are obtained are labelled.

Table 2: Individual Steps of Our Algorithm Presented in a Structured Outline [11]

Outline of Approach		
1	Input image and filter twice with 4x4 median filter to reduce speckle noise	
2	Filter each column with the second derivative of Gaussian, acting as a one dimensional edge detection kernel	
3	Choose the strongest two edges, scaled by relative contrast, as the initial approximation to the inner and outer boundaries.	
4	Segment the initial approximations at boundary discontinuities	
5	Build a continuous boundary from the segments. Start with the longest segment, and first move left and then move right. As boundaries are found, they are considered to be "determined."	
	5a	Try to link either the initial inner or outer boundary in the new segment with the previous, determined, segment.
	5b	Use the Markov model to find the correct inner and/or outer boundary in the new segment if it cannot be linked with those in determined segments.
	5c	Check the results of the Markov model for blunders. If blunders are detected, use the original boundaries.
6	Once a continuous boundary is detected, smooth it with a cubic B-spline.	

Table 2 outlines the individual steps in the algorithm for clarification. It is important to note that although the Markov model parameters are established through a statistical evaluation, once set these parameters are kept constant. Thus, for a given B-scan, the algorithm always produces the same result. Initially a 4 X 4 median filter is applied twice to each image to suppress the speckle noise. Most of the speckle is removed, while the gross retinal outlines are intact. For finite impulse response edge-detection kernel, a 1-D Gaussian second derivative was used. These edge detectors step response is a zero crossing whose slope and polarity vary with contrast and polarity of the step.
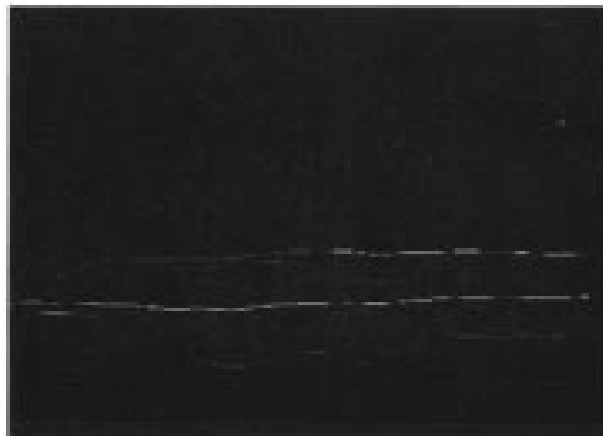
Figure 11: Edges Found by the Edge Detector [11]

The upper and lower retinal boundaries in Figure 11 are, for the most part, the brightest edges in each column. The initial boundary estimate relies on this general trend by choosing, for each A-scan, the brightest two edges separated by at least ten pixels. Initial boundary contours were broken into segments bordered by vertical dislocations larger than ten pixels in *either* contour. The next step is to complete and refine the inner and outer retinal boundaries using information from the Markov model and as much of the initial approximation as possible. Three distinct cases can occur when extending a boundary between segments and in each case, it is determined if either contour in the new segment is continuous with a boundary in the neighbouring determined segment.

The initial boundary approximations were segmented at discontinuities and so at least one segment contour will always fail the ten-pixel criterion for continuity. At this point, a fairly accurate boundary description of the retina has been set. Although a Markov model of the retinal structure is invoked, it is used to select from existing edge responses and not to interpolate between edges or to correct edge positions. According to the initial assumption the retinal boundary must be smooth, so a final spline-based adjustment is applied. The centroids of each consecutive (non overlapping) group of three boundary points are computed.

The retinal thickness values resulting from the boundaries rather than directly assessing the boundary were evaluated. The boundaries determined by the algorithm generally followed the retinal contours extremely well; the deviations that did occur were most commonly in the outer retinal boundary. Most scans required very little or no correction, as in others suffered noticeable dips or rises in the boundaries, causing larger errors. The incidence of each error type is presented in Table IV for the new algorithm.

Table 3: Summary of Errors in Determination of Average Retinal Thickness for the New Algorithm [11]

Error Type	Training Set (330 Scans)		Entire Data Set (1450 Scans)	
	Whole Scan ROI	33 Column ROI	Whole Scan ROI	33 Column ROI
Insignificant	99.7%	83.0%	97.0%	73.6%
Small	0.3%	16.7%	3.0%	24.8%
Large	0	0.3%	0	1.6%
Failure	0		0.1%	

The incidence of each error type is presented in Table 3 for the new algorithm. The results for the entire set of 1450 images are listed as well as the results from the set of 330 training images.

Our algorithm determines retinal thickness with an error comparable to the 10- m fundamental OCT resolution and reported intersession repeatability for the vast majority of the 1450 OCT images. Most of the remaining errors were still less than 10% of normal retinal thickness and, thus, represent a substantial improvement over current clinical measurements. There were four basic sources of error.

- The large amount of speckle noise was not completely removed by median filtering and induced many spurious edges.

- The median filtering introduces its own errors as well, by erasing small image features and blurring some of the small discontinuities between adjacent A-scans.

- Furthermore, the 1-D edge detector selects the leading edges of the retinal boundary peaks.

- There was a discrepancy between the retinal boundary model used for the algorithm design and the edges chosen for the hand corrections. Retinal boundaries in OCT images were assumed to be edges featuring large intensity gradients and lying below very dark regions.

The contribution in this paper can perhaps best be characterized as the first, fundamental building block in a complete OCT retinal analysis system, based on a sophisticated mathematical model of retinal structure.

3. RESULTS

The detection of the retinal fiber layer thickness from an OCT image is important for the diagnosis of glaucoma. Three measurement techniques have been reviewed.

Gaussian Mixture Model is an automatic hybrid framework which can accurately and stably segment eight retinal layers with nine boundaries. The basic idea that the intensity change is highest at the middle of the interface between the layers is the concept used to detect difficult boundaries. A method that tracks the changes between neighbouring pixels using two masks is developed to overcome the problems of image degradation, such as excessive speckle noise and low image contrast. A major disadvantage of GMM clustering is that spatial dependences are not taken into account. However, kernels naturally include spatial dependences.

The proposed technique for automated layer segmentation first detects the retinal blood vessels and accordingly cuts an OCT image into multiple vessel sections and non-vessel sections. The non-vessel sections are then smoothed by a bilateral filter and a median filter. Finally, retinal layer boundaries of the smoothed non-vessel sections are detected and the complete retinal layer boundaries are determined through interpolation.

The retinal boundary-detection system described in Markov Boundary detection determines the average retinal thickness to accuracy comparable to the machine resolution for the vast majority of OCT images. Reliable and accurate measurements of retinal thickness can be expected to improve both the clinical usefulness of the OCT, as well as patient care.

4. CONCLUSIONS

In ophthalmology quantitative analysis of retinal structures is important for estimating pathological changes and diagnosing retinal diseases using OCT, which is an optical signal acquisition and processing method where, the resolution achieved is of the order of micrometer and the images are three-dimensional in nature. Glaucoma characterized by the loss of the retinal nerve fiber can be diagnosed by measuring the retinal nerve fiber layer (RNFL) thickness within OCT images. Of the three techniques reviewed the GMM gives eight retinal layers with nine boundaries and is therefore more reliable, accurate and has a higher computational speed than the other two methods.

REFERENCES

1. D. Huang, E. A. Swanson, C. P. Lin, J. S. Schuman, W. G. Stinson, W. Chang, M. R. Hee, T. Flotte, K. Gregory, C.A. Puliafito, and J. G. Fujimoto, "Optical coherence tomography," Science 254(5035), 1178–1181 (1991).

2. W. M. Hart, "Adler's physiology of the eye," in *Mosby Year Book*, 9th ed., W. M. Hart, Ed. Chicago, IL, 1992.

3. F. Ferris and A. Patz, "Macular edema: A complication of diabeticretinopathy," *Survey Ophthalmol.*, vol. 28S, pp. 452–461, 1984.

4. "Photocoagulation for diabetic macular edema: Early treatment diabetic retinopathy study report," *Int. Ophthalmol. Clin.*, vol. 27, pp. 265–271, 1987.

5. D. Huang, E. A. Swanson, and C. P. Lin *et al.*, "Optical coherence tomography," *Science*, vol. 254, pp. 1178–1181, 1991.

6. T. M. Nguyen and Q. M. J. Wu, "Dirichlet Gaussian mixture model: Application to image segmentation," *Image Vis. Comput.*, vol. 29, no. 12, pp. 818–828, 2011.

7. M. Thune, B. Olstad, and N. Thune, "Edge detection in noisy data using finite mixture distribution analysis," *Pattern Recogn.*, vol. 30, pp. 685–699, 1997.

8. N. Otsu, "A threshold selection method from gray-level histogram," *IEEE Tran. Syst., Man, Cybern.*, vol SMC-19, no. 1, pp. 62–66, Jan. 1979.

9. J. Canny, "A computational approach to edge detection," *IEEE Trans. Pattern Anal. Mach. Intell.*, vol. PAMI-8, no. 6, pp. 679–714, Nov. 1986.

10. Lu Shijian, Cheung Yim-luiCarol, Liu Jiang, J. H. Lim, C. Kai-shun Leung, and T. Y. Wong "Automated Layer Segmentation of Optical Coherence Tomography Images, "IEEE Trans. BioMed. Engg., vol. 57, no. 10, pp. 2605–2608, Oct. 2010.

11. *Koozekanani Dara, Kim Boyer*,"* Retinal Thickness Measurements From Optical Coherence Tomography Using a Markov Boundary Model. IEEE Trans. Med. Img., vol. 20, no. 9, pp. 900–916, Sep. 2001.

12. Yeong-Mun Cha and Jae-Ho Han*, "*High-Accuracy Retinal Layer Segmentation for Optical Coherence Tomography Using Tracking Kernels Based on Gaussian Mixture Model*"*. IEEE Journal of selected topics in Quantum Electronics, vol. 20, no. 2, pp. 6801010, March/April. 2014.